Published in final edited form as:
J Neuroophthalmol. 2012 September ; 32(3): . doi:10.1097/WNO.0b013e3182589589.

Neuronal Programmed Cell Death-1 Ligand Expression Regulates Retinal Ganglion Cell Number in Neonatal and Adult Mice

Caroline W. Sham, MD, PhD, **Ann M. Chan, MS**, **Jacky M. K. Kwong, PhD**, **Joseph Caprioli, MD**, **Steven Nusinowitz, PhD**, **Bryan Chen, BS**, **Janice G. Lee, MD**, **Nishant M. Gandhi, MD**, **Loise M. Francisco, PhD**, **Arlene H. Sharpe, MD, PhD**, **Ling Chen, MD, PhD**, **Jonathan Braun, MD, PhD**, and **Lynn K. Gordon, MD, PhD**

Departments of Pathology and Laboratory Medicine (CWS, JB) and Ophthalmology (AMC, JMKK, JC, SN, BC, JGL, NMG, LKG), Jules Stein Eye Institute, David Geffen School of Medicine, University of California Los Angeles, Los Angeles, California; Department of Pathology (LMF, AHS), Harvard Medical School, Boston, Massachusetts; Department of Pathology (LMF, AHS), Brigham and Women's Hospital, Boston, Massachusetts; Department of Ophthalmology (LC), Eye and ENT Hospital, Shanghai Medical School, Fudan University, Shanghai, China; and Ophthalmology Section (LKG), Greater Los Angeles Veterans Affairs Healthcare System, Los Angeles, California.

Abstract

Objectives—During mouse retina maturation, the final number of retinal ganglion cells (RGCs) is determined by highly regulated programmed cell death. Previous studies demonstrated that the immunoregulatory receptor programmed cell death-1 (PD-1) promotes developmental RGC death. To identify the functional signaling partner(s) for PD-1, we identified retinal expression of PD-1 ligands and examined the effect of PD-1 ligand expression on RGC number. We also explored the hypothesis that PD-1 signaling promotes the development of functional visual circuitry.

Methods—Characterization of retinal and brain programmed cell death-1 ligand 1 (PD-L1) expression were examined by immunofluorescence on tissue sections. The contribution of PD-ligands, PD-L1, and programmed cell death-1 ligand 2 (PD-L2) to RGC number was examined in PD-ligand knockout mice lacking 1 or both ligands. Retinal architecture was assessed by spectral-domain optical coherence tomography, and retinal function was analyzed by electroretinography in wild-type and PD-L1/L2 double-deficient mice.

Results—PD-L1 expression is found throughout the neonatal retina and persists in adult RGCs, bipolar interneurons, and Müller glia. In the absence of both PD-ligands, there is a significant numerical increase in RGCs (34% at postnatal day 2 [P2] and 18% in adult), as compared to wild type, and PD-ligands have redundant function in this process. Despite the increased RGC number, adult PD-L1/L2 double-knockout mice have normal retinal architecture and outer retina function.

Conclusion—This study demonstrates that PD-L1 and PD-L2 together impact the final number of RGCs in adult mice and supports a novel role for active promotion of neuronal cell death through PD-1 receptor-ligand engagement.

Address correspondence to Lynn K. Gordon, MD, PhD, Jules Stein Eye Institute, David Geffen School of Medicine at UCLA, 100 Stein Plaza, Los Angeles, CA 90095; lgordon@mednet.ucla.edu.

The authors declare no conflict of interest.

In the developing central nervous system (CNS), many more neurons are created than are necessary to form functional circuits. Excess neurons are eliminated by carefully regulated apoptotic programmed cell death (PCD) in a process called developmental cell death (1). Murine postnatal retina maturation is an example of ontogenic cell death, providing a model to study PCD in the CNS (2). PCD has been particularly explored well in retinal ganglion cells (RGCs), as about half of RGCs born will die by this process (3). To survive and form functional circuitry, RGCs must project axons to the brain, synapse on target cells, and avoid elimination by synaptic pruning (2). A variety of cell surface interactions are known to positively and negatively influence this developmental sequence. Cell surface adhesion γ-protocadherin proteins (4), neurotrophic support (5), and electrical activity (6) are all required for proper RGC survival. In contrast to these influences, molecules decorating cell processes, such as complement initiating factor C1q (7), CD3ζ, and MHCI (8) and neuronal pentraxins (9), act to promote synaptic refinement. Additionally, the p75NTR neurotrophin (10) and programmed cell death-1 (PD-1) (11) receptors act to promote RGC death.

PD-1 is a membrane-associated coinhibitory receptor, expressed on a number of hematopoietic cells including T cells, B cells, and macrophages (12) and on neurons of the CNS (11,13). In the immune system setting, PD-1 engagement with 1 of the 2 ligands, PD-L1 or PD-L2, acts to attenuate immune responses and thus has broad immunoregulatory roles in peripheral tolerance, as well as immunity to chronic infections, tumors, and organ transplants (12). We previously reported that PD-1 receptor ligation promotes RGC apoptosis during early postnatal development and identified PD-L1 and PD-L2 gene expression throughout retina maturation (11), suggesting that either one or both PD-ligands engage functionally with PD-1 in the retina. In this study, we identify the cellular expression of PD-ligand proteins and demonstrate an increased RGC number in the absence of PD-L1 and PD-L2.

METHODS

Animals

Knockout mice were constructed in the C57BL/6 background, as previously described: PD-1$^{-/-}$, PD-L1$^{-/-}$, PD-L2$^{-/-}$, and PD-L1/L2$^{-/-}$ (14-16). Animals used for each experiment are described in Table 1. Wild-type (WT) embryonic and adult age-matched C57BL/6 mice were purchased from Charles River Laboratory. All animal experiments were reviewed and approved by the University of California, Los Angeles, Chancellor's Animal Research Committee, in adherence to the Association for Research in Vision and Ophthalmology Statement for the Use of Animals in Ophthalmic and Vision Research.

Animal Perfusion

Mice were deeply anesthetized with intraperitoneal sodium pentobarbital (80 mg/kg of Nembutal) and perfused transcardially with 10 mL of 4% paraformaldehyde (PFA) in phosphate buffered saline (PBS) for 5 minutes.

Immunofluorescence Staining

Paraformaldehyde-fixed, frozen vertical retina sections of 7-μm thickness were prepared from postnatal day 2 (P2) and adult (P56) animals. Staining and epifluorescent imaging were performed as previously described (11). Antibodies used, including PD-L2 antibodies tested, are listed in Table 2. For brain sections, adult (P56) WT male mice were perfused, brains were dissected, postfixed in 4% PFA/PBS overnight at 4°C, cryoprotected in 30% sucrose/PBS, and embedded in optical coherence tomography (OCT) medium (Sakura Finetek). Serial coronal sections of 25 μm were collected at the level of the superior colliculus (SCs) at Bregma −4.1 to −4.4 mm; coordinates were determined using the Allen Mouse Brain

reference atlas (26). Immunofluorescence staining was performed for PD-1 and PD-L1, using the same method as for retina sections, with the exception that all slide washing was performed with agitation.

Optic Nerve Axon Analysis

Adult (P28) WT, PD-1$^{-/-}$, and PD-L1/L2$^{-/-}$ mice were perfused. Optic nerves were dissected, postfixed in 1% osmium tetraoxide, stained with 1% potassium ferricyanide, dehydrated in ethanol and acetone, and embedded in epoxy resin. Ultrathin (70 nm) optic nerve sections were obtained with a microtome (Reichert Ultracut) at approximately 400 mm posterior to the eye globe, placed on slotted grids, and counterstained with 1% uranyl acetate and Sato lead. Images were obtained using transmission electron microscopy (Tecnai; FEI). For each section, 20 micrographs were taken at ×21,000 at representative optic nerve regions: central (4), midperipheral (8), and peripheral (8). No positional adjustments were made. Images included blood vessels and glial cells. Micrographs were digitized using a 2K chargecoupled device (Photometrics Inc). Analysis was performed according to published methods (27).

Semi-thin (1 μm) optic nerve sections were stained with 1% toluidine blue (Sigma Aldrich). To determine axon density, axons located within a counting frame (8 × 8 μm) and intersecting the upper and right frame edges were counted manually in a blinded manner. Mean axon density was calculated as total axons divided by total area.

Nissl Staining

To stain all neuronal cell bodies, every fourth coronal brain section was Nissl stained as previously described (28), with 0.1% cresyl violet (Sigma-Aldrich). Structures were localized using Nissl stains in conjunction with the Allen Mouse Brain reference atlas (26).

Imaging and Quantification of Immunofluorescence Staining

Retina sections were imaged at ×400 magnification, yielding an image width of 262 μm. Quantification of ganglion cell layer (GCL) cell types, RGCs and displaced amacrine cells, and statistical analysis were performed as previously described (11). Semithin optic nerve sections were imaged at ×400 magnification, and cross-sectional area was measured by outlining the nerve border with image acquisition software (DP2-BSW, Olympus) and repeated on 3 consecutive sections. Brain sections were imaged at ×100 magnification. All images were obtained with light or epifluorescent microscopy (BX51, Olympus).

Retina Architecture

Following euthanasia, eyes were rapidly enucleated and immediately fixed in 4% PFA. Paraffin embedding, sectioning at 4 μm thickness, and hematoxylin and eosin (H&E) staining were performed by UCLA's Translational Pathology Core Laboratory (TPCL). Images were obtained at ×400 magnification by light microscopy, as above.

Electroretinogram

Adult (6 week-old) WT and PD-L1/L2$^{-/-}$ male mice were dark-adapted overnight for full-field flash electroretinogram (ERG) recording as previously described (29). Briefly, ERGs were recorded using a gold electrode touching the corneal surface referenced to a gold electrode in the mouth. Scotopic rod-mediated responses were obtained to blue flashes (Wratten 47A, λ_{max} = 470 nm, Eastman Kodak). After a 5-minute light adaptation, cone-mediated responses were recorded. Analysis was performed using custom software (29). Amplitude of dark-adapted *b* wave was plotted against flash intensity and resulting

intensity-response function was fit with a Naka-Rushton equation to derive V_{max} (maximum saturated amplitude) and k (semisaturation intensity.)

Spectral-Domain Optical Coherence Tomography

Spectral-domain OCT (SD-OCT) imaging (Bioptigen) was performed. Animals were anesthetized and left pupils dilated with atropine (1% wt/vol atropine sulfate ophthalmic solution). Recordings were taken with a 50° field of view, yielding a 1.5-mm-diameter image. En face view C-scans were recorded with the optic nerve head (ONH) centered in the image and consisted of 100 two-dimensional B-scans, which in turn consisted of 800 one-dimensional A-scans. Total scan time was approximately 5 seconds. Retinal layers were measured at 0.2 mm eccentricity from the ONH with analysis software (Software Suite; Bioptigen). At 0.6 mm eccentricity from the ONH, in both temporal and superior orientations, no differences were noted between WT and PD-L1/L2$^{-/-}$ total retina thickness ($P = 0.83$ and 0.43, respectively), thus representative central measurements are reported. Retina layer analysis was performed referencing published mouse OCT images (30). “Inner retina” was defined as the distance from the inner limiting membrane to the inner nuclear layer (INL), and “outer retina” was defined as the distance from the outer plexiform layer (OPL) to the retinal pigment epithelium.

Statistical Analysis

A graphing program (Prism 5; GraphPad) was used for data visualization and statistical analysis. For immunofluorescence quantification, optic nerve axon counts, and retina architecture analysis, a Student t test was used to compare groups. For ERG data, mean and standard error of the mean (SEM) were plotted at each frequency, and Boltzmann sigmoidal curves were fitted to the data. For scotopic ERG, an unpaired t test was used to compare V_{max} and k between WT and PD-L1/L2$^{-/-}$ mice. For timing and photopic ERG amplitude, 2-way analysis of variance was used to evaluate difference between WT and PD-L1/L2$^{-/-}$ mice.

RESULTS

PD-L1 Is Expressed in RGCs, Bipolar Interneurons, and Müller Glia of the Mature Mouse Retina

Retinal expression of *Pdcd1lg1* (PD-L1 gene) has been reported (11), identifying it as a neuronal PD-ligand. To determine potential locations for PD-1 ligation, PD-L1 protein localization was characterized in the mouse retina and SCs, the major target of rodent optic nerve axons (31). During postnatal retina maturation, a wave of RGC death occurs, peaking at P2–P5 (32). At P2, coincident with this peak, PD-L1 expression is found in the GCL in a nonnuclear distribution and in the neuroblast layer distributed on the neuropil colocalizing with PD-1 receptor expression (Fig. 1A). In addition, PD-L1 is expressed in cell processes of the incipient inner plexiform layer (Fig. 1A). In the mature retina, PD-L1 expression persists and is restricted to the inner retina layers (Fig. 1B). Since PD-L1 was found across the INL, inner plexiform layer, and GCL, immunofluorescence (IF) double labeling with GCL and INL cell type markers was performed. PD-L1 was found to be expressed in many but not all cell types. PD-L1 expression did not colocalize with 2 types of interneurons: AP2α-positive amacrine cells and calbindin D28K-positive horizontal cells (Fig. 1B). However, PD-L1 expression did colocalize with 2 neuronal cell types: Brn3a-positive RGCs, and both protein kinase C (PKC) α-positive rod bipolar axon terminals and Goα-positive optical nerve (ON) bipolar dendrites, and in addition, 1 glial cell type: glutamine synthetase-positive Müller cell bodies and processes (Fig. 1B). Within the OPL, PD-L1 expression was observed at ON cone bipolar terminals of cone pedicle synapses, as evidenced by colocalization with the ON bipolar marker Goα, which labels both ON cone

and rod bipolars (33) but not with the rod bipolar marker PKCα. Although neuronal *Pdcd1lg2* (PD-L2 gene) expression has been previously described (11), PD-L2 protein expression was below the threshold of detection by IF using several anti-PD-L2 antibodies (Table 2).

Since RGCs express both PD-1 and PD-L1 and extend axons to the brain via the optic nerve, we next explored expression of the PD-1 signaling system in the superficial layers of the SCs, the location to which the majority of mouse RGCs project (31). Both PD-1 and PD-L1 are expressed across the SCs, including the stratum opticum, which contains afferent optic nerve fibers of RGCs (Fig. 1C, D). This expression pattern supports the possibility that PD-1:PD-L1 engagement can also occur at the axon terminals of RGCs. Within the SCs, higher resolution imaging will be necessary to determine the subcellular localization of PD-1 and PD-L1 and also the spatial relationship of cells expressing each molecule.

Absence of Both PD-Ligands Results in Persistent Increase in RGC Number

To test the importance of PD-L1 GCL expression during peak RGC apoptosis, we next tested the functional role of PD-ligands in developmental RGC death and predicted that similar to that reported previously for PD-1 receptor knockout (PD-$1^{-/-}$) mice (11), the genetic absence of PD-ligands would increase RGC survival in the neonatal period. GCL layer compartments were assessed during the development of the PD-L1 and PD-L2 double-knockout (PD-L1/$L2^{-/-}$) mouse retina, in comparison to WT controls, by immunofluorescent staining for the RGC and amacrine cell markers Brn3a and AP2α, respectively (Fig. 2A). At P2, the PD-L1/$L2^{-/-}$ retina has a significant increase in RGC number compared to WT (34 ± 2.9%; $P = 0.006$; Fig. 2B), measured by the number of Brn3a-positive nuclei per millimeter. Given that these observations for PD-L1/$L2^{-/-}$ mirror the previously reported PD-$1^{-/-}$ phenotype (11), we were surprised to observe that in contrast to the PD-$1^{-/-}$ adult retina, PD-L1/$L2^{-/-}$ adult retinas have a significant increase in RGC number compared to WT (18 ± 5.4%; $P = 0.04$; Fig. 2C). To confirm this increase, optic nerve axon counting was performed and showed that adult PD-L1/$L2^{-/-}$ had significantly increased mean axon density, as compared to WT (Fig. 3C; $P = 0.01$). To determine which PD-ligand contributes to the adult phenotype, we examined retinas from single PD-ligand knockouts, PD-$L1^{-/-}$, and PD-$L2^{-/-}$ and found that neither had a difference in RGC number as compared to WT ($P = 0.07$ and 0.14, respectively; Fig. 2C). A significant number of displaced amacrine cells also reside in the GCL (34), so we also examined amacrine cell number in the absence of PD-1 ligation. In the adult retina, there were no significant differences in amacrine cell number between any of the knockout strains, as compared to WT ($P \geq 0.4$ for all knockout strains; Fig. 2D). These findings suggest that PD-L1 and PD-L2 have redundant roles in RGC cell death, and their concurrent absence is associated with a persistent increase in RGC number of the mature retina.

Normal Gross Retina Architecture and Function in the PD-L1/$L2^{-/-}$ Adult Mouse

The observed increase in the numbers of RGCs in the PD-L1/$L2^{-/-}$ animals prompted further evaluation of the functional significance of this observation. We first explored if the normal highly organized, laminated retina structure was present in the mature adult PD-L1/$L2^{-/-}$ retina by H&E stain and found the gross architecture to be normal, as compared to WT (Fig. 4A). Retina architecture of 6-week-old PD-L1/$L2^{-/-}$ and WT mice was visualized in vivo by SD-OCT. Reconstructed vertical sections (Fig. 4B, D) and en face fundus images (Fig. 4C, E) both appeared grossly normal in PD-L1/$L2^{-/-}$ mice (Fig. 4D, E). There were no significant differences in inner or outer retina layer thickness between PD-L1/$L2^{-/-}$ and WT (Fig. 4F, G), and concordantly, no significant differences when either the inner (Figs. 3, 4H) or outer (Figs. 3, 4I) retina was broken down to nuclear and nonnuclear layer components.

Since we observed PD-L1 expression colocalizing with PKCα-positive rod bipolar axon terminals and Goα-positive ON bipolar dendrites, we next investigated middle and outer retina function using standard ERG. Representative ERGs recorded from PD-L1/L2$^{-/-}$ mice are shown in Figure 5A. No statistically significant differences in rod-mediated retinal function were observed between PD-L1/L2$^{-/-}$and WT adult mice (Fig. 5B, C), although the PD-L1/L2$^{-/-}$ demonstrated a weak trend in the direction of reduced response amplitude (V_{max}) and photoreceptor sensitivity (k) ($P = 0.68$ for V_{max} and $P = 0.07$ for k; Fig. 5B). Correspondingly, there were no statistically significant differences in cone-mediated function (Fig 5C; $P = 0.46$). Finally, we analyzed the timing of peak components of the rod-mediated and cone-mediated ERGs and found no statistically significant differences ($P =$ 0.16 and 0.71, respectively). These data collectively demonstrate that retinal structure and outer retinal function are both normal in adult PD-L1/L2$^{-/-}$ mice.

DISCUSSION

Developmental RGC death in mice is a highly regulated process, generating the correct number of surviving RGCs necessary to form functional connections with the optic tectum and visual cortex (3). According to the neurotrophic hypothesis, RGC death results from the lack of available extracellular neurotrophic support (35). The discovery of a neurotrophic death–promoting signal, nerve growth factor engagement with p75NTR, introduced the additional hypothesis that soluble neurotrophic ligands can provide an active death trigger for retinal neurons (36). Our work introduces an important refinement to this idea, where receptor engagement with a cell-associated ligand can also promote developmental RGC death. We refer to this hypothesis as “active selection” of neuronal elimination.

PD-1 ligation blockade in vitro was found to decrease RGC apoptosis during peak RGC death (11), supporting a role for PD-1 receptor-ligand interaction in this process. This work, summarized in Table 1, presents strong evidence that PD-1 ligands, PD-L1, and PD-L2 are the functional neuronal ligands for PD-1, acting within the GCL to influence RGC-specific developmental cell death. Furthermore, PD-L1 is expressed in the developing and mature retina, suggesting potential for engagement with PD-1 receptor during these times. We hypothesize several potential locations for PD-1 ligation within the retina. First, developmental ligation between GCL cell types could lead to cell death. Second, in the mature retina, PD-L1 on rod bipolar could potentially interact with PD-1 on AP2α-positive glycinergic AII amacrine cells (11,37). Third, PD-L1 on Müller glia, which ensheath all retinal cell types (38), could engage PD-1–positive RGCs and/or amacrine cells (11). PD-L1 expression at cone bipolar terminals suggests a potential role for PD-L1 in cone pathway visual responses. The presence of PD-L1 in the mature retina, along with PD-1 receptor (11), suggests additional roles for PD-1 ligation beyond developmental RGC cell death. Since the PD-L1/L2$^{-/-}$ retina has normal gross function by ERG, PD-ligands are not required for wiring functional circuitry within the retina. Further studies are necessary to assess whether PD-1 ligation has a role in defining retina-brain projections, perhaps through synaptic refinement, similar to other cell surface immune molecules in the CNS (8).

Perturbations of neurotrophic support (39-41), neurotrophic death (10,42), or PD-1 signaling (11) cause transient changes in RGC survival in vivo. However, none of these cell surface survival modulators are sufficient to influence the final number of RGCs in the mature adult retina. Here, we provide the first evidence for a receptorligand signal having a more persistent effect on RGC numbers. Genetic absence of both PD-ligands yields an 18% increase in RGCs in the mature retina. However, this difference is modest compared to inactivation of intracellular apoptotic machinery, where RGC numbers can be increased 50%–226%, as reviewed (3).

The observation that the absence of both PD-ligands had a persistent effect on RGC survival, while the absence of PD-1 receptor only has a transient early developmental effect (11) led us to hypothesize the presence of another neuronal PD-ligand receptor functioning during the final phase of developmental cell death. One strong candidate is another B7 family costimulatory ligand B7-1, shown to interact with PD-L1 (but not PD-L2) in lymphocytes, with ligation resulting in similar immunoinhibitory effects as PD-1 ligation (43). Defining additional PD-ligand interacting molecules in the retina, including B7-1, and which elicit an “active selection” death signal are questions for future investigation.

PD-L1 expression in Müller glia is intriguing, as this cell type has both protective and detrimental roles in retinal disease (44). We hypothesize that PD-1 ligation could act to downregulate Müller glia activity in settings of retinal damage. Although PD-L1 expression was characterized in this study, we were unable to reliably detect PD-L2 protein expression by immunofluorescence in the developing and mature mouse retina. Genetic evidence that PD-L2 is functionally redundant with PD-L1 in promoting RGC death, in combination with identification of PD-L2 gene expression, will require further characterization of neuronal PD-L2 protein expression. In summary, our work solidifies the role of PD-ligands in RGC developmental cell death and provides impetus to explore the role of the PD-1 signaling pathway in neurodegenerative retinal disease.

Acknowledgments

The authors thank Dr. Xian-Jie Yang for valuable discussions throughout this work, Dr Gordon Freeman for the gift of the PD-1 monoclonal antibody, Marianne Cilluffo at the UCLA Brain Research Institute Electron Microscopy core laboratory for extensive tissue processing and imaging assistance, and the UCLA Translational Pathology Core Laboratory for tissue processing assistance. The 3B5 monoclonal antibody, developed by T. Williams was obtained from the Developmental Studies Hybridoma Bank developed under the auspices of the National Institute of Child Health and Human Development and maintained by The University of Iowa, Department of Biology, Iowa City, Iowa.

This work was supported by the UCLA Medical Scientist Training Program NIH T32 GM08042 (CWS), National Institutes of Health/National Institute of Allergy and Infectious Diseases Grant RO1 AI021256 (CWS), JSEI Vision Science Training Grant NIH/NEI T32 EY007026 (CWS), P01AI56299 (AHS), Pujiang Talent Foundation 10PJ1401900 (LC), and National Science Foundation of China 81000381 (LC).

REFERENCES

1. Blomgren K, Leist M, Groc L. Pathological apoptosis in the developing brain. Apoptosis. 2007; 12:993–1010. [PubMed: 17453164]
2. Vecino E, Hernandez M, Garcia M. Cell death in the developing vertebrate retina. Int J Dev Biol. 2004; 48:965–974. [PubMed: 15558487]
3. Isenmann S, Kretz A, Cellerino A. Molecular determinants of retinal ganglion cell development, survival, and regeneration. Prog Retin Eye Res. 2003; 22:483–543. [PubMed: 12742393]
4. Lefebvre JL, Zhang Y, Meister M, Wang X, Sanes JR. Gamma-protocadherins regulate neuronal survival but are dispensable for circuit formation in retina. Development. 2008; 135:4141–4151. [PubMed: 19029044]
5. Farah MH. Neurogenesis and cell death in the ganglion cell layer of vertebrate retina. Brain Res Rev. 2006; 52:264–274. [PubMed: 16764935]
6. Goldberg JL, Espinosa JS, Xu Y, Davidson N, Kovacs GT, Barres BA. Retinal ganglion cells do not extend axons by default: promotion by neurotrophic signaling and electrical activity. Neuron. 2002; 33:689–702. [PubMed: 11879647]
7. Stevens B, Allen NJ, Vazquez LE, Howell GR, Christopherson KS, Nouri N, Micheva KD, Mehalow AK, Huberman AD, Stafford B, Sher A, Litke AM, Lambris JD, Smith SJ, John SW, Barres BA. The classical complement cascade mediates CNS synapse elimination. Cell. 2007; 131:1164–1178. [PubMed: 18083105]

8. Boulanger LM, Shatz CJ. Immune signalling in neural development, synaptic plasticity and disease. Nat Rev Neurosci. 2004; 5:521–531. [PubMed: 15208694]
9. Bjartmar L, Huberman AD, Ullian EM, Renteria RC, Liu X, Xu W, Prezioso J, Susman MW, Stellwagen D, Stokes CC, Cho R, Worley P, Malenka RC, Ball S, Peachey NS, Copenhagen D, Chapman B, Nakamoto M, Barres BA, Perin MS. Neuronal pentraxins mediate synaptic refinement in the developing visual system. J Neurosci. 2006; 26:6269–6281. [PubMed: 16763034]
10. Harada C, Harada T, Nakamura K, Sakai Y, Tanaka K, Parada LF. Effect of p75NTR on the regulation of naturally occurring cell death and retinal ganglion cell number in the mouse eye. Dev Biol. 2006; 290:57–65. [PubMed: 16343477]
11. Chen L, Sham CW, Chan AM, Francisco LM, Wu Y, Mareninov S, Sharpe AH, Freeman GJ, Yang XJ, Braun J, Gordon LK. Role of the immune modulator programmed cell death-1 during development and apoptosis of mouse retinal ganglion cells. Invest Ophthalmol Vis Sci. 2009; 50:4941–4948. [PubMed: 19420345]
12. Keir ME, Butte MJ, Freeman GJ, Sharpe AH. PD-1 and its ligands in tolerance and immunity. Annu Rev Immunol. 2008; 26:677–704. [PubMed: 18173375]
13. Chen L, Pai V, Levinson R, Sharpe AH, Freeman GJ, Braun J, Gordon LK. Constitutive neuronal expression of the immune regulator, programmed death 1 (PD-1), identified during experimental autoimmune uveitis. Ocul Immunol Inflamm. 2009; 17:47–55. [PubMed: 19294574]
14. Keir ME, Freeman GJ, Sharpe AH. PD-1 regulates self-reactive CD8+ T cell responses to antigen in lymph nodes and tissues. J Immunol. 2007; 179:5064–5070. [PubMed: 17911591]
15. Keir ME, Liang SC, Guleria I, Latchman YE, Qipo A, Albacker LA, Koulmanda M, Freeman GJ, Sayegh MH, Sharpe AH. Tissue expression of PD-L1 mediates peripheral T cell tolerance. J Exp Med. 2006; 203:883–895. [PubMed: 16606670]
16. Latchman YE, Liang SC, Wu Y, Chernova T, Sobel RA, Klemm M, Kuchroo VK, Freeman GJ, Sharpe AH. PD-L1-deficient mice show that PD-L1 on T cells, antigen-presenting cells, and host tissues negatively regulates T cells. Proc Natl Acad Sci U S A. 2004; 101:10691–10696. [PubMed: 15249675]
17. Liang SC, Latchman YE, Buhlmann JE, Tomczak MF, Horwitz BH, Freeman GJ, Sharpe AH. Regulation of PD-1, PD-L1, and PD-L2 expression during normal and autoimmune responses. Eur J Immunol. 2003; 33:2706–2716. [PubMed: 14515254]
18. Liu W, Khare SL, Liang X, Peters MA, Liu X, Cepko CL, Xiang M. All Brn3 genes can promote retinal ganglion cell differentiation in the chick. Development. 2000; 127:3237–3247. [PubMed: 10887080]
19. West-Mays JA, Zhang J, Nottoli T, Hagopian-Donaldson S, Libby D, Strissel KJ, Williams T. AP-2alpha transcription factor is required for early morphogenesis of the lens vesicle. Dev Biol. 1999; 206:46–62. [PubMed: 9918694]
20. Dyer MA, Livesey FJ, Cepko CL, Oliver G. Prox1 function controls progenitor cell proliferation and horizontal cell genesis in the mammalian retina. Nat Genet. 2003; 34:53–58. [PubMed: 12692551]
21. Haverkamp S, Ghosh KK, Hirano AA, Wassle H. Immunocytochemical description of five bipolar cell types of the mouse retina. J Comp Neurol. 2003; 455:463–476. [PubMed: 12508320]
22. Hernandez M, Rodriguez FD, Sharma SC, Vecino E. Immunohistochemical changes in rat retinas at various time periods of elevated intraocular pressure. Mol Vis. 2009; 15:2696–2709. [PubMed: 20019879]
23. Dhingra A, Lyubarsky A, Jiang M, Pugh EN Jr, Birnbaumer L, Sterling P, Vardi N. The light response of ON bipolar neurons requires G[alpha]o. J Neurosci. 2000; 20:9053–9058. [PubMed: 11124982]
24. Linser PJ, Sorrentino M, Moscona AA. Cellular compartmentalization of carbonic anhydrase-C and glutamine synthetase in developing and mature mouse neural retina. Brain Res. 1984; 315:65–71. [PubMed: 6144368]
25. Morrow EM, Chen CM, Cepko CL. Temporal order of bipolar cell genesis in the neural retina. Neural Dev. 2008; 3:2. [PubMed: 18215319]
26. Lein ES, Hawrylycz MJ, Ao N, Ayres M, Bensinger A, Bernard A, Boe AF, Boguski MS, Brockway KS, Byrnes EJ, Chen L, Chen TM, Chin MC, Chong J, Crook BE, Czaplinska A, Dang

CN, Datta S, Dee NR, Desaki AL, Desta T, Diep E, Dolbeare TA, Donelan MJ, Dong HW, Dougherty JG, Duncan BJ, Ebbert AJ, Eichele G, Estin LK, Faber C, Facer BA, Fields R, Fischer SR, Fliss TP, Frensley C, Gates SN, Glattfelder KJ, Halverson KR, Hart MR, Hohmann JG, Howell MP, Jeung DP, Johnson RA, Karr PT, Kawal R, Kidney JM, Knapik RH, Kuan CL, Lake JH, Laramee AR, Larsen KD, Lau C, Lemon TA, Liang AJ, Liu Y, Luong LT, Michaels J, Morgan JJ, Morgan RJ, Mortrud MT, Mosqueda NF, Ng LL, Ng R, Orta GJ, Overly CC, Pak TH, Parry SE, Pathak SD, Pearson OC, Puchalski RB, Riley ZL, Rockett HR, Rowland SA, Royall JJ, Ruiz MJ, Sarno NR, Schaffnit K, Shapovalova NV, Sivisay T, Slaughterbeck CR, Smith SC, Smith KA, Smith BI, Sodt AJ, Stewart NN, Stumpf KR, Sunkin SM, Sutram M, Tam A, Teemer CD, Thaller C, Thompson CL, Varnam LR, Visel A, Whitlock RM, Wohnoutka PE, Wolkey CK, Wong VY, Wood M, Yaylaoglu MB, Young RC, Youngstrom BL, Yuan XF, Zhang B, Zwingman TA, Jones AR. Genome-wide atlas of gene expression in the adult mouse brain. Nature. 2007; 445:168–176. [PubMed: 17151600]

27. Mabuchi F, Aihara M, Mackey MR, Lindsey JD, Weinreb RN. Optic nerve damage in experimental mouse ocular hypertension. Invest Ophthalmol Vis Sci. 2003; 44:4321–4330. [PubMed: 14507876]
28. Paxinos, G.; Halliday, G.; Watson, C.; Koutcherov, Y.; Wang, HQ. Atlas of the Developing Mouse Brain. 1st edition. Elsevier; New York, NY: 2007.
29. Jin M, Li S, Nusinowitz S, Lloyd M, Hu J, Radu RA, Bok D, Travis GH. The role of interphotoreceptor retinoid-binding protein on the translocation of visual retinoids and function of cone photoreceptors. J Neurosci. 2009; 29:1486–1495. [PubMed: 19193895]
30. Fischer MD, Huber G, Beck SC, Tanimoto N, Muehlfriedel R, Fahl E, Grimm C, Wenzel A, Reme CE, van de Pavert SA, Wijnholds J, Pacal M, Bremner R, Seeliger MW. Noninvasive, in vivo assessment of mouse retinal structure using optical coherence tomography. PLoS One. 2009; 4:e7507. [PubMed: 19838301]
31. Hofbauer A, Drager UC. Depth segregation of retinal ganglion cells projecting to mouse superior colliculus. J Comp Neurol. 1985; 234:465, 474. [PubMed: 3988995]
32. Young RW. Cell death during differentiation of the retina in the mouse. J Comp Neurol. 1984; 229:362–373. [PubMed: 6501608]
33. Vardi N, Dhingra A, Zhang L, Lyubarsky A, Wang TL, Morigiwa K. Neurochemical organization of the first visual synapse. Keio J Med. 2002; 51:154–164. [PubMed: 12371647]
34. Perez De Sevilla Muller L, Shelley J, Weiler R. Displaced amacrine cells of the mouse retina. J Comp Neurol. 2007; 505:177–189. [PubMed: 17853452]
35. Oppenheim RW. Cell death during development of the nervous system. Ann Rev Neurosci. 1991; 14:453–501. [PubMed: 2031577]
36. Frade JM, Rodríguez-Tébar A, Barde Y-A. Induction of cell death by endogenous nerve growth factor through its p75 receptor. Nature. 1996; 383:166–168. [PubMed: 8774880]
37. Bassett EA, Pontoriero GF, Feng W, Marquardt T, Fini ME, Williams T, West-Mays JA. Conditional deletion of activating protein 2alpha (AP-2alpha) in the developing retina demonstrates non-cell-autonomous roles for AP-2alpha in optic cup development. Mol Cell Biol. 2007; 27:7497–7510. [PubMed: 17724084]
38. Bringmann A, Pannicke T, Grosche J, Francke M, Wiedemann P, Skatchkov SN, Osborne NN, Reichenbach A. Muller cells in the healthy and diseased retina. Prog Retin Eye Res. 2006; 25:397–424. [PubMed: 16839797]
39. Pollock GS, Robichon R, Boyd KA, Kerkel KA, Kramer M, Lyles J, Ambalavanar R, Khan A, Kaplan DR, Williams RW, Frost DO. TrkB receptor signaling regulates developmental death dynamics, but not final number, of retinal ganglion cells. J Neurosci. 2003; 23:10137–10145. [PubMed: 14602830]
40. Cellerino A, Carroll P, Thoenen H, Barde YA. Reduced size of retinal ganglion cell axons and hypomyelination in mice lacking brain-derived neurotrophic factor. Mol Cell Neurosci. 1997; 9:397–408. [PubMed: 9361277]
41. Rohrer B, LaVail MM, Jones KR, Reichardt LF. Neurotrophin Receptor TrkB activation is not required for the postnatal survival of retinal ganglion cells in vivo. Exp Neurol. 2001; 172:81–91. [PubMed: 11681842]

42. Frade JM, Barde YA. Genetic evidence for cell death mediated by nerve growth factor and the neurotrophin receptor p75 in the developing mouse retina and spinal cord. Development. 1999; 126:683–690. [PubMed: 9895316]

43. Butte MJ, Keir ME, Phamduy TB, Sharpe AH, Freeman GJ. Programmed death-1 ligand 1 interacts specifically with the B7-1 costimulatory molecule to inhibit T cell responses. Immunity. 2007; 27:111–122. [PubMed: 17629517]

44. Bringmann A, Iandiev I, Pannicke T, Wurm A, Hollborn M, Wiedemann P, Osborne NN, Reichenbach A. Cellular signaling and factors involved in Müller cell gliosis: neuroprotective and detrimental effects. Prog Retin Eye Res. 2009; 28:423–451. [PubMed: 19660572]

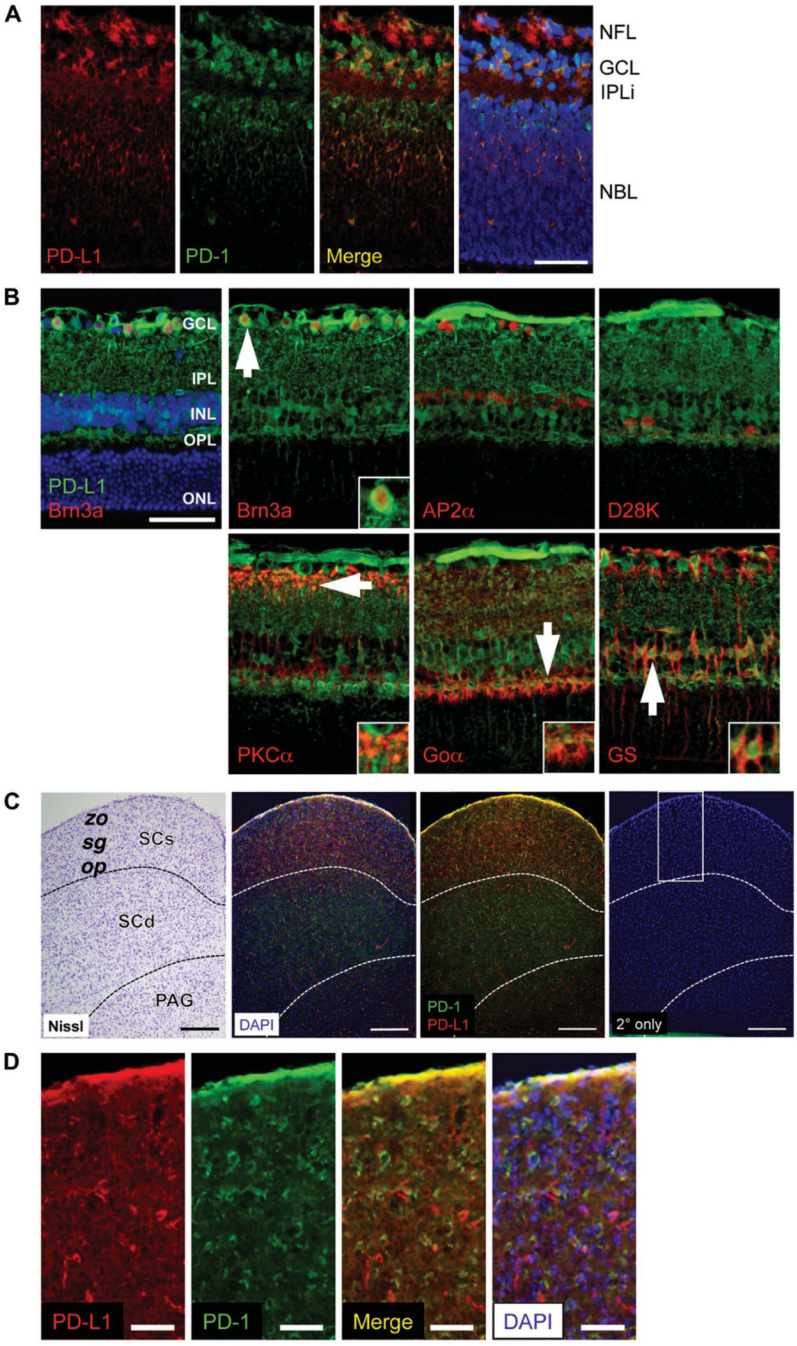

FIG. 1.

PD-L1 expression in the neonatal mouse retina and brain by immunofluorescence staining. **A**. PD-1 (green) and PD-L1 (red) expression at P2 in the central retina, at the level of the optic nerve. **B**. PD-L1 (green) and the following retinal cell type markers (all in red): Brn3a for RGCs, AP2α for amacrine cells, Calbindin D28K (D28K) for horizontal cells, PKCα for rod bipolar cells, Goα for optic nerve bipolar cells, glutamine synthetase (GS) for Müller glia. *White arrows* indicate cells shown at higher magnification inset into each panel. All images were taken at the level of the optic nerve, at the midpoint between the optic nerve head (ONH) and periphery. **C**. Coronal section of the superior colliculus at Bregma −4.3

mm, after Allen Mouse Brain Atlas coordinates. Panels from left to right show: 1) Nissl stain, 2) PD-1 (green) and PD-L1 (red) expression by immunofluorescence, with DAPI counterstain (blue), 3) same as second image, without DAPI, and 4) secondary only negative control, where PD-1 and PD-L1 primary antibodies were omitted, and the white box indicates area shown at higher magnification in **D**. **D**. Higher magnification of SCs. Panels from left to right show: 1) PD-L1 (red) expression, 2) PD-1 (green) expression, 3) PD-L1 and PD-1 expression colocalization (yellow), and 4) PD-L1 and PD-1 expression with DAPI (blue) counterstain. Scale bars = 50 μm (**A**, **B**, **D**) and 200 μm (**C**). For each expression pattern shown, 3 animals were examined. Nuclei were visualized with DAPI (blue) counterstain. Yellow represents colocalization of PD-1 and PD-L1. GCL, ganglion cell layer; INL, inner nuclear layer; IPL, inner plexiform layer; IPLi, incipient inner plexiform layer; NBL, neuroblast layer; NFL, nerve fiber layer; ONL, outer nuclear layer; OPL, outer plexiform layer; *op*, stratum opticum; PAG, periaqueductal gray; SCs, superior colliculus superficial layers; SCd, superior colliculus, deep layers; *sg*, stratum griseum superficiale; *zo*, stratum zonale.

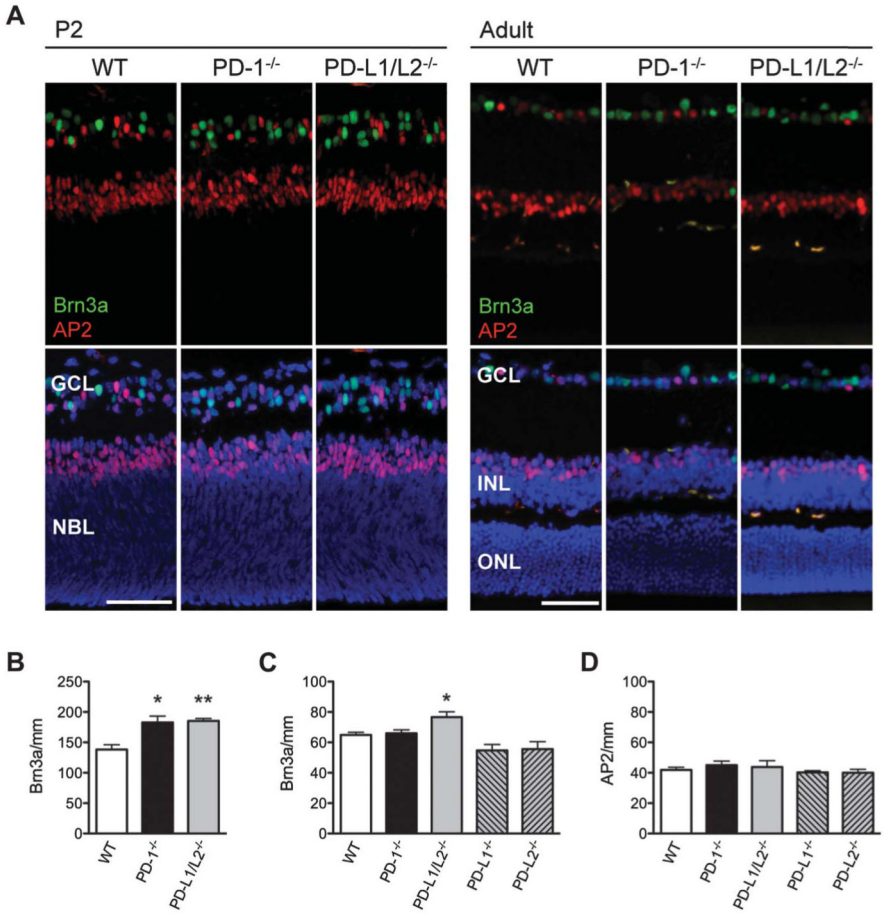

FIG. 2.

Increased RGCs in the neonatal and adult retina of PD-L1/L2$^{-/-}$ mice. **A**. Immunofluorescence staining for Brn3a (green) and AP2α (red) in P2 and adult (P56) retina of WT, PD-1$^{-/-}$, and PD-L1/L2$^{-/-}$ mice, with DAPI nuclear counterstain (blue). Scale bars = 50 μm. **B**. Quantification of RGC number (Brn3a/mm) in WT, PD-1$^{-/-}$ mice at P2. Quantification of RGC number (Brn3a/mm, **B**, **C**) and amacrine cell number (AP2/mm, **D**) in the adult retina. Three mice per strain were analyzed at each time point. For each quantified readout, the mean and standard error of the mean were plotted. *Significant *P* value in comparing each knockout to WT; *$P \leq 0.04$, **$P = 0.006$.

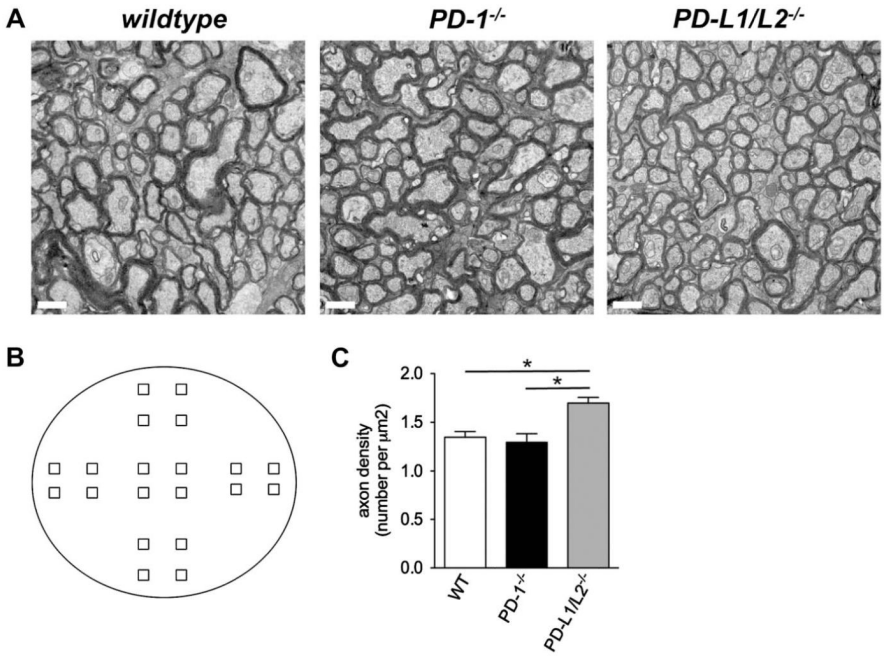

FIG. 3.

Optic nerve axon analysis in PD-1 and PD-ligand knockout mice. **A**. Electron micrographs (×21,000) of the central region. Scale bars are 1 μm. **B**. Optic nerve cross-sectional area: WT (53,624 ± 982), PD-$1^{-/-}$ (52,865 ± 2137), and PD-L1/$L2^{-/-}$ (48,008 ± 363). **C**. Total axon number: WT (72,107 ± 2113), PD-$1^{-/-}$ (68,141 ± 3574), PD-L1/$L2^{-/-}$ (81,658 ± 3356) (**P* = 0.05). **D**. Axon density: WT (1.35 ± 0.057), PD-$1^{-/-}$ (1.29 ± 0.089), PD-L1/$L2^{-/-}$ (1.70 ± 0.059), **P* = 0.01 (WT vs PD-L1/$L2^{-/-}$), *P* = 0.02 (PD-$1^{-/-}$ v. PD-L1/$L2^{-/-}$). **E**. Schematic representation of location for 20 micrographs taken from each nerve. Central region includes the 4 squares at the center, peripheral region includes the 8 outer most squares, and midperipheral region includes the 8 remaining squares. **F**. Central region axon number: WT (17,901 ± 582), PD-$1^{-/-}$ (17,337 ± 1409), PD-L1/$L2^{-/-}$ (20,158 ±1081). **G**. Central region axon density: WT (0.334 ± 0.015), PD-$1^{-/-}$ (0.329 ± 0.031), PD-L1/$L2^{-/-}$ (0.419 ± 0.020), **P* = 0.03.

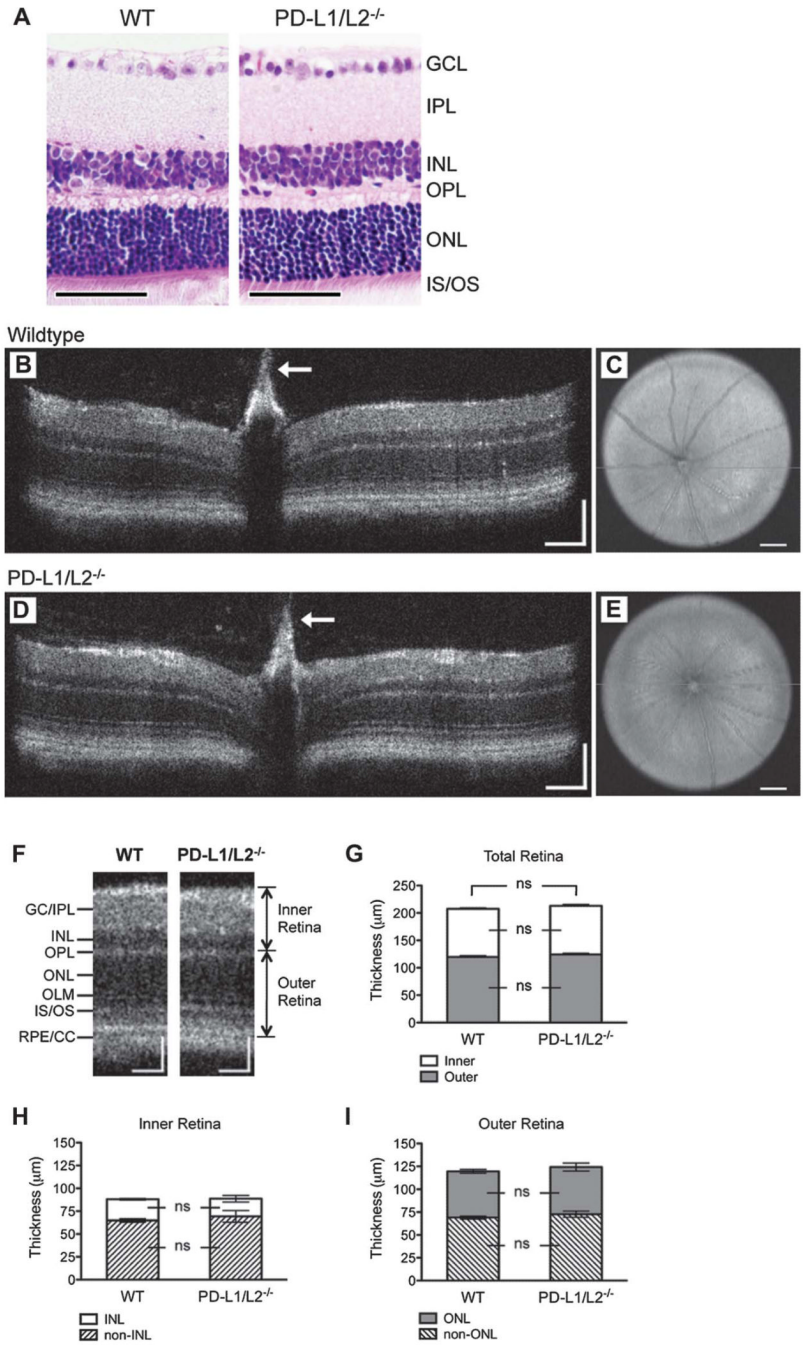

FIG. 4.

Retina architecture in PD-1 and PD-ligand knockout mice. **A**. Hematoxylin and eosin stain showing gross retina architecture of WT and PD-L1/L2$^{-/-}$ adult mice. Representative B-scan images at the level of the optic nerve head showing a retina crosssection from WT (**B**) and PD-L1/L2$^{-/-}$ (**D**) mice. White arrows indicate Bergmeister papilla, a remnant of fetal hyaloid vasculature commonly observed in C57BL/6 mice on spectral-domain optical coherence tomographic imaging. Representative en face C-scans showing fundus images from WT (**C**) and PD-L1/L2$^{-/-}$ (**E**) mice, with the horizontal green line indicating orientation of respective B-scans. F. Cropped view of WT (**B**) and PD-L1/L2$^{-/-}$ (**D**) B-

scans, labeled to indicate retinal layers and landmarks used for quantification of layer thickness. Quantification of inner, outer, and total retina thickness (**G**), and nuclear layer and nonnuclear layer components of the inner or outer retina (**H** or **I**, respectively). GC/IPL, ganglion cell and inner plexiform layers; INL, OPL, ONL, as defined above in Fig. 1; IS/OS, photoreceptor inner and outer segments; OLM, outer limiting membrane; ns, not significant; RPE/CC, retinal pigment epithelium and choriocapillaris. Scale bars = 50 μm (A), 100 μm (both *x*- and *y*-axes, B, D, F), or 200 μm (C, E).

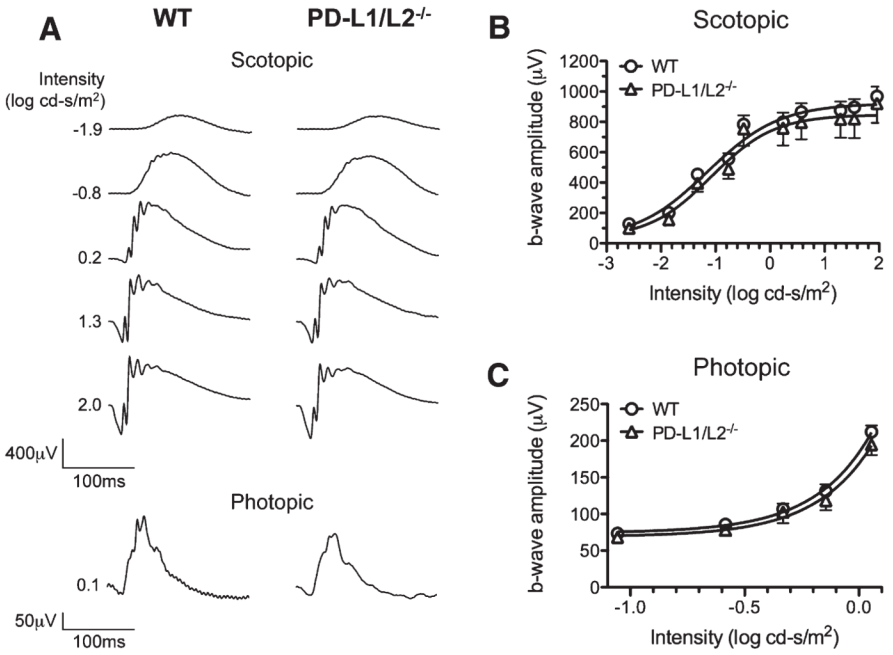

FIG. 5.

PD-L1/L2$^{-/-}$ mice have normal outer retina function. **A**. Representative raw electroretinogram traces for WT and PD-L1/L2$^{-/-}$ mice. Maximum *b*-wave amplitude in PD-L1/L2$^{-/-}$ (n = 3, open triangles) and WT (n = 5, open circles) mice, over a range of stimulus intensities, for both scotopic (**B**) and photopic (**C**) conditions. Amplitudes are presented as mean ± standard error of the mean. Scotopic response characteristics for WT: V_{max} = 883.6 ± 60.1 μV, k = 0.055 ± 0.003 c-s/m^2; and for PD-L1/L2$^{-/-}$: V_{max} = 832.5 ± 122.1 μV, k = 0.066 ± 0.004 c-s/m^2.

TABLE 1

Summary of experimental animal (mice) studies showing the effect of programmed cell death-1 ligands on retinal ganglion cell number

Experiment	Strain	Age	Age Rationale	Result
Retinal PD-L1 expression by IF	WT	P2	Age-match RGC quantification	Expressed in GCL cell bodies and neuroblast layer neuropil
	WT	P56	Age-match brain expression	Expressed in RGCs, bipolar cells, and Müller glia
Brain PD-1 and PD-L1 expression by IF	WT	P56	Age-matched to reference mouse brain atlas (ref)	PD-1 and PD-L1 expressed in SCs
RGC quantification by IF	WT	P2	Peak RGC death	Increased RGC number in PD-$1^{-/-}$ and PD-L1/$L2^{-/-}$
	PD-$1^{-/-}$			
	PD-L1/L2"/-			
	WT	P56	Age-match brain expression	Increased RGC number in PD-L1/$L2^{-/-}$
	PD-$1^{-/-}$			
	PD-L1/$L2^{-/-}$			
	PD-$L1^{-/-}$			
	PD-$L2^{-/-}$			
Axon counting by electron microscopy	WT	P28	Establish baseline for future experiments	Increased RGC number in PD-L1/$L2^{-/-}$
	PD-$1^{-/-}$			
	PD-L1/$L2^{-/-}$			
ERG and SD-OCT	WT	P42	Knockout animal availability	Normal outer retina function and architecture in PD-$1^{-/-}$ and PD-L1/$L2^{-/-}$
	PD-$1^{-/-}$			
	PD-L1/$L2^{-/-}$			

TABLE 2

Primary antibodies used for immunofluorescence staining (13,17-25).

Antibody	Dilution	Source
Anti-mouse PD-1 (clone 29F.1A12, rat IgG2α) (17)	1:200	Gift of Gordon Freeman, MD, PhD (Boston, MA)
Anti-PD-L1/CD274 (rabbit polyclonal) (17)	1:750	Lifespan Biosciences, #LS-B480
Anti-mouse Brn3a (clone 5A 3.2, mouse IgG1) (18)	1:200	Millipore/Chemicon
Anti-mouse AP2a (clone 3B5, mouse IgG2β) (19)	1:20	Developmental Studies
Hybridoma Bank		
Anti-Calbindin D28K (clone CB-955 (formerly CL-300), mouse IgG1) (20)	1:1000	Sigma-Aldrich
Anti-PKCa (clone H-7, mouse IgG1) (21,22)	1:4000	Santa Cruz Biotechnology
Anti-G protein Goa (clone 2A, mouse IgG1) (23)	1:1000	Millipore/Chemicon
Anti-glutamine synthetase (clone GS-6, mouse IgG2α) (24,25)	1:1000	Millipore/Chemicon
Species- or isotype-specific Alexa Fluor 488 or 594	1:1000	Invitrogen
Anti-mouse PD-L2 (clone TY25, rat IgG2α) (13,17)	—	eBioscience
Anti-mouse PD-L2 (clone 19G.4H3, rat IgG2β)	—	Gift of Gordon Freeman, MD, PhD (Boston, MA)
Anti-human PD-L2 (clone 24F.7G12, mouse IgG2α)	—	Gift of Gordon Freeman, MD, PhD (Boston, MA)